International Journal of Structural Stability and Dynamics
(2023) 2350117 (27 pages)

DOI: 10.1142/S0219455423501171

World Scientific
www.worldscientific.com

A Novel Regularized Adaptive Matching Pursuit for Moving Force Identification Using Multiple Criteria and Prior Knowledge

Bohao Xu and Ling Yu*

MOE Key Laboratory of Disaster Forecast and Control in Engineering
School of Mechanics and Construction Engineering
Jinan University, Guangzhou 510632, P. R. China
**lyu1997@163.com*

Received 7 September 2022
Accepted 12 November 2022
Published

Moving force identification (MFI) is one of the challenging tasks in structural health monitoring (SHM) of bridges. As an inverse problem, continuous attention is needed to address the ill-posedness of MFI system matrix, computational efficiency and accuracy. Therefore, a novel regularized adaptive matching pursuit (NRAMP) framework is proposed for MFI using multiple criteria and prior knowledge in this study. Firstly, a relationship between moving forces and structural responses is established. With the utilization of redundant matrix, the MFI problem is converted into one of the sparse recoveries. A new adaptive criterion related to atoms both in the sparse regularization and LSQR factorization is introduced into the regularized orthogonal matching pursuit (ROMP) process. The ill-posedness of system matrix in sparse recovery can be reduced greatly, and the unknown sparsity problem can be skipped. Furthermore, the optimal atoms of redundant matrix will be selected repeatedly based on another criterion related to prior knowledge that the static axle-weight of a vehicle is the main component of moving vehicle force. The residual in each iteration will be saved and the atoms with the smallest residual are chosen at last. Finally, to assess the feasibility of the proposed method, numerical simulations on identification of single moving force with impulse components and two unequal moving forces, and experimental verifications on MFI of a model vehicle moving on a beam in laboratory are also carried out. The results show that the relative percentage errors between the identified and true gross vehicle weight keep under 3.6% in all measured cases, and the executive time of the proposed method is far less than that due to common OMP methods.

Keywords: Moving force identification (MFI); structural health monitoring (SHM); redundant concatenated dictionary; sparse regularization; matching pursuit; vehicle–bridge interaction.

1. Introduction

Moving forces, such as highway vehicles or railway trains, as main loadings acting on the bridge deck, have been extensively studied in the field of structural health

*Corresponding author.

monitoring (SHM) recently.[1,2] They have been adopted not only for bridge design but also for extraction of bridge information and structural damage identification.[3–6] However, they are hard to be directly identified so there have been lots of indirect methods proposed based on structural responses caused by moving forces. Furthermore, direct identification methods need to consume much in materials, manpower and financial resources compared with indirect methods. For indirect methods, the earlier researchers concentrated on the establishment of relationship between moving forces and structural responses.[7–13] In general, they can be divided into two categories by the models used.[7] One is the discrete finite element (FE) model-based method,[8,9] and the other is the analytical model-based method. Based on the classical theories, the latter is more accurate than the former if the model is established in an ideal condition. There are lots of outstanding jobs in the analytical model-based method, such as time domain method (TDM),[10] frequency domain method,[11] second interpretation[12] and state space method.[13] Among them, the TDM is relatively accurate than the other methods.[14] Therefore, most of the subsequent investigations are based on the TDM, and the moving force identification (MFI) problem is converted into a linear inverse problem with an ill-posedness. Due to these characteristics, the solution to the MFI is very sensitive and easy to be polluted by noise. Then some regularization methods are widely adopted to tackle these weaknesses.

The traditional Tikhonov method has been widely used to settle the ill-posed problem. It assumes that the solution is stable so that a penalty term, so-called l_2-norm regularization term, is added to the solution to the linear inverse problem.[15] Zhu and Law[16,17] introduced the regularization into the MFI and the results show that the Tikhonov method can improve the accuracy of the existing methods. However, since the Tikhonov matrix is selected as the identity matrix, the MFI result is usually smooth and overfitted.[18]

To overcome the weakness mentioned above, the sparse regularization method had been introduced into interface force identification.[19] However, it should be noted that the sparse regularization method cannot be directly used in MFI. This is because moving forces are not to be zeros within the whole time history in time domain when they are moving across the bridge deck. It is assumed that the force time history can be constructed by a sum of weighted basis functions.[19–21] Therefore, the solution accuracy is largely determined by the matching degree of real engineering problem and choice of weighted basis functions.[22] Furthermore, the chosen atoms by different methods are also a significant problem in MFI based on redundant matrix.[23] Pan *et al.*[24] proposed an alternative method based on redundant concatenated dictionary, where the basis functions in the redundant concatenated dictionary were assumed as trigonometric functions and rectangular functions used to describe the periodic and impulse features of moving forces greatly. Finally, the solution to MFI was obtained by the fast iterative shrinkage-thresholding algorithm (FISTA), which is a common solution to the l_1-norm regularization method. In Refs. 25–27, the sparse solutions were obtained with the utilization of same l_1-norm regularization

method or its improved versions, and the identified results showed great. However, the l_1-norm regularization penalty is still difficult to be chosen even though there are lots of different ways,[28] such as Akaike information criterion (AIC), Bayesian information criterion (BIC), cross validation (CV) and so on. Furthermore, even though the executive time of the FISTA is short, the l_1-norm regularization penalty is time-consuming to be obtained and will be changed in different response cases. Matching pursuit (MP) is also a classical choice for the sparse solution.[29] However, its performance is not so great in real engineering problem. Therefore, orthogonal matching pursuit (OMP) has been introduced to force identification.[30] Even though the OMP is transparent: a new coordinate is selected from the support of the original signal in a natural and specific way at each iteration, it has relatively weak guarantee for accurate recovery compared with l_1-minimization.[31] Therefore, there are some other improved algorithms based on OMP, such as regularized orthogonal matching pursuit (ROMP) algorithm which has been proven that its executive time is much shorter than the OMP in the real engineering problem and that the strong uniform guarantees of l_1-minimization.[32] However, there are still some tricky problems for these matching pursuit algorithms when they are introduced into MFI. Firstly, the sparsity of MFI problem is unknown, and it is hard for some matching pursuit algorithms, such as ROMP, to be used directly. Secondly, MFI is an ill-posed problem, and it is hard to solve the MFI for these algorithms by direct matrix inversion (DMI). Thirdly, unlike the l_1-norm regularization penalty which can consider the prior knowledge that a moving vehicle loading consists of static axle-weight and dynamic load components, in which the former accounts for most of them, these matching pursuit algorithms are hard to take this relationship.

To tackle these problems, a novel regularized adaptive matching pursuit (NRAMP) is proposed for the MFI based on multiple criteria and prior knowledge in this study. This algorithm can save the regularization of the ROMP algorithm. To solve the unknown sparsity problem, a novel adaptive criterion related to the regularized process is proposed. The adaptive criteria related to the residual, which is a common process to solve the unknown sparsity problem,[33,34] is also combined with this novel criterion. However, because the measured data is polluted by noise, there will probably be no atoms selected in regularized process even though the residual does not meet the requirements of adaptive criteria with the increase of iterations. Therefore, an adaptive criterion in regularized process is necessary. To solve the problems related to the ill-posedness and the utilization of prior knowledge, the LSQR method is chosen to solve the least square problem to tackle the ill-posed problem instead of DMI method in each matching pursuit iteration.[35] The obtained results in each iteration are also filtered by a proposed criterion related to the prior knowledge, which is that the static axle-weight is the main component of gross vehicle weight of a vehicle. Furthermore, the final results are chosen by the minimum residual in all iterations to assure that the selected atoms are the best choice. Through these criteria and initiatives, the MFI results will be more accurate and

have stronger robustness, and simultaneously they can conform to another prior knowledge that the dynamic components of each moving force fluctuate around the static component in it.

The structure of this paper is organized as follows. In Sec. 2, the theoretical background of the proposed NRAMP is introduced. Some numerical simulations on identification of different moving forces, such as single moving force with impulse components and two unequal moving forces, are carried out in Sec. 3. Furthermore, to assess the adaptabilities of the NRAMP, experimental verifications are conducted through identifying loadings of a model vehicle moving on a hollow thin-wall beam in Sec. 4. Finally, some conclusions are drawn in Sec. 5.

2. Theoretical Background

2.1. *Time domain method*

As shown in Fig. 1, a simply-supported beam is taken as an example to establish the relationship between structural responses and a moving force. The bridge parameters are as follows: EI is flexural rigidity, c is viscous damping parameter, l is the length of beam, and ρ is mass per unit length. Furthermore, $\chi_n(x)$ and $q_n(t)$ are the mode shape function of the nth mode and the nth modal amplitudes, respectively. The time history of the force is more concerned, and it is considered as a function only with respect to time. The speed of the moving force is v. Then the equation of the bridge–vehicle system can be written by the mode superposition approach as follows[10]:

$$\ddot{q}_n(t) + 2\xi_n \dot{q}(t) + \omega_n^2 q_n(t) = \frac{2}{\rho l} P_n(t) \quad (n = 1, 2, \ldots, \infty), \tag{1}$$

where $\omega_n = n^2\pi^2/l^2\sqrt{EI/\rho}$, $\xi_n = c/2\rho\omega_n$, $P_n(t) = P(t)\chi_n(x_p)$ and x_p means the location of the moving force on the bridge.

Considering that the moving force is a step function in a small-time interval, the relationship between structural responses and moving force can be established. Then the structural responses of both bending moment and acceleration responses can be

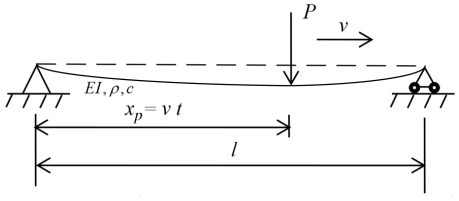

Fig. 1. Simply-supported beam subjected to a moving force.

combined:

$$\begin{bmatrix} \dfrac{\boldsymbol{C}_1}{\|\boldsymbol{m}\|} \\ \dfrac{\boldsymbol{C}_2}{\|\boldsymbol{a}\|} \end{bmatrix} \boldsymbol{P} = \begin{bmatrix} \dfrac{\boldsymbol{m}}{\|\boldsymbol{m}\|} \\ \dfrac{\boldsymbol{a}}{\|\boldsymbol{a}\|} \end{bmatrix}, \tag{2}$$

where matrixes $\boldsymbol{C}_1$ and $\boldsymbol{C}_2$ are system matrixes between force $\boldsymbol{P}$ and bending moment $\boldsymbol{m}$ and between force $\boldsymbol{P}$ and acceleration response $\boldsymbol{a}$, respectively, and $\|\cdot\|$ is a vector norm.

Moreover, Eq. (2) can be briefly rewritten as

$$\boldsymbol{JP} = \boldsymbol{Y}, \tag{3}$$

where $\boldsymbol{J}$ is a normalized system matrix with a dimension of $n_r \times n_f$, $\boldsymbol{P}$ is a vector of moving force with a dimension of $n_f \times 1$ and $\boldsymbol{Y}$ is a vector of normalized responses with a dimension of $n_r \times 1$.

2.2. *Moving force expression by redundant dictionaries*

Based on the theory of redundant dictionaries, moving force P can be expressed using basis function in a matrix-vector form:

$$\boldsymbol{P} = \boldsymbol{W}\boldsymbol{\alpha}, \tag{4}$$

where $\boldsymbol{W}$ is a redundant dictionary which is expressed by

$$\boldsymbol{W} = [\phi_1, \phi_2, \ldots, \phi_N],$$

and it is also a square orthogonal matrix. $\boldsymbol{\alpha}$ is a coefficient vector of the redundant dictionary $\boldsymbol{W}$, and it can be expressed by

$$\boldsymbol{\alpha} = [\alpha_1, \alpha_2, \ldots, \alpha_N]^T.$$

The subscript N is the number of employed basis functions, which is important in redundant dictionary theory. To be convenient, the number of basis functions for each moving force is the same.

For the choice of basis functions, sines and cosines, spline functions, etc., are widely used.[25] An appropriate basis function is significant for the expression of moving force.[22] Therefore, the redundant dictionary in Ref. 24, which is constructed with the trigonometric and rectangular functions, is used in this study. According to prior knowledge, the moving force consists of static and dynamic components. The static component can be described by a constant vector which is related to the first atom in the redundant matrix. For the dynamic components which consist of the periodic and local impulse components of moving forces, they can be well described by the trigonometric and rectangular functions, respectively. Then according to the prior knowledge that the static axle-weigh component of a vehicle accounts for majority of gross vehicle weight (GVW), the coefficient related to this atom should be larger than the others.

The number of basis functions is also a significant factor in the accuracy of moving force. The number of basis functions is estimated below according to Ref. 24:

$$n_r = n_t = \lfloor 2 \times T \times f_r + 0.5 \rfloor, \tag{5}$$

where n_r and n_t are the number of rectangular and trigonometric functions, respectively, T is the time spent that a moving force goes across the bridge, f_r is the highest interested frequency of unknown moving forces, and $\lfloor\ \rfloor$ is an operation which rounds down the value to the nearest integer.

Substituting Eq. (4) into Eq. (3), a new equation between moving force and bridge responses can be established as follows:

$$\boldsymbol{JW}\boldsymbol{\alpha} = \boldsymbol{Y}. \tag{6}$$

For brevity, $\boldsymbol{JW}$ is expressed as a new matrix $\boldsymbol{\Phi}$, then Eq. (6) can be rewritten as

$$\boldsymbol{\Phi}\boldsymbol{\alpha} = \boldsymbol{Y}. \tag{7}$$

2.3. *Novel regularized adaptive matching pursuit*

From the previous sections, it is easy to be found that the $\boldsymbol{\alpha}$ is a sparse vector due to the redundant dictionary. Then the solution to Eq. (7) can be considered as an unconstrained optimization problem:

$$\min \|\boldsymbol{\Phi}\|_1, \text{s.t.},\ \|\boldsymbol{\Phi}\boldsymbol{\alpha} - \boldsymbol{Y}\|_2. \tag{8}$$

In this study, a novel regularized adaptive matching pursuit (NRAMP) method, which is based on the regularized orthogonal matching pursuit (ROMP), is proposed to tackle this problem. Therefore, before introducing the NRAMP method, the process of the ROMP is summarized as follows[31]:

Initialize: Set index set $\boldsymbol{I} = \emptyset$, initial update matrix $\boldsymbol{A} = \emptyset$ and initial residual $\boldsymbol{r} = \boldsymbol{Y}$, then repeat the following steps until $|\boldsymbol{I}| \geq 2s$ or the maximum iteration s. Here, s is the sparsity of $\boldsymbol{\alpha}$.

Identify: Calculate $\boldsymbol{u} = \boldsymbol{\Phi}^T\boldsymbol{Y}$, and then choose the n biggest coordinates in magnitude of $\boldsymbol{u}$. If the number of the nonzero coordinate is smaller than n, all the nonzero coordinates should be chosen. Find the corresponding vector in $\boldsymbol{\Phi}$ to organize a new set $\boldsymbol{Q}$.

Regularize: Let the subset $\boldsymbol{Q}_0 \subset \boldsymbol{Q}$ which has the maximum value $\boldsymbol{u}_{\max}$ of $\sum_j |\boldsymbol{u}(j)|^2$, where j represents the number of vectors chosen in the subset $\boldsymbol{Q}_0$.

Update: Add the best choice in *Regularize* to the index set $\boldsymbol{I} = \boldsymbol{I} \cup \boldsymbol{Q}_0$, and construct update matrix: $\boldsymbol{A} = \boldsymbol{A} \cup \boldsymbol{\Phi}_{\boldsymbol{Q}_0}$. Then set all the elements of $\boldsymbol{\Phi}_{\boldsymbol{Q}_0}$ in $\boldsymbol{\Phi}$ as zero:

$$\boldsymbol{\Phi}_{\boldsymbol{Q}_0} = \boldsymbol{\Theta}, \tag{9}$$

where $\boldsymbol{\Phi}_{\boldsymbol{Q}_0}$ and $\boldsymbol{\Theta}$ represent the column vectors in $\boldsymbol{\Phi}$ related to $\boldsymbol{Q}_0$ and a matrix or a vector with all zero values, respectively.

And then calculate the least square function:

$$\boldsymbol{\alpha}_i = \arg\min_{\boldsymbol{\zeta}\in\mathbb{R}^I} \|\boldsymbol{Y} - \boldsymbol{A}\boldsymbol{\zeta}\|. \tag{10}$$

It should be noted that direct matrix inversion (DMI) is used in the solution to Eq. (9).

Then update the residual:

$$\boldsymbol{r} = \boldsymbol{Y} - \boldsymbol{A}\boldsymbol{\alpha}_i, \tag{11}$$

where i is the current number of iterations.

Output: Combine the $\boldsymbol{\alpha}_i$ in each iteration to obtain a reconstructed answer.

It can be found that there are some problems that need to be solved before this algorithm is introduced into MFI. In the first process, the sparsity of the coefficient should be known. Secondly, the coefficients related to the chosen index will be changed with the increase of iteration, which means that the residual may not be the smallest in the final iteration. Thirdly, Eq. (8) should be solved carefully due to the ill-posedness of the MFI. Fourthly, prior knowledge that the static axle-weight component of a vehicle mainly contributes to the GVW is not reflected in it.

Regarding these problems, a novel regularized adaptive matching pursuit (NRAMP) method is proposed to address them, some improvements are enhanced here in the following procedures.

According to the unknown sparsity problem, some adaptive processes are proposed in Refs. 33 and 34. However, these modifications are only linked to the residual in one iteration. For the MFI problem, the noise always has a great impact on the identified results, the related parameters of atoms are smaller compared to the moving force. Therefore, based on the adaptive process about the residual, two iteration stopping criteria are established to solve the unknown sparsity problem. One stopping criterion as in Ref. 33 is still used here. When the updated residual $\boldsymbol{r}$ in the process of *Update* is smaller than ε_1, the iteration would be stopped. Furthermore, another stopping criterion is proposed to solve the problem of noise. When the maximum value $\boldsymbol{u}_{\max}$ in the process of *Regularize* is smaller than ε_2, the algorithm will also be stopped. This process assures that the most chosen atom is not related to noise even though the stopping criterion about the residual is not reached.

For the second problem, it should be noted that the reason for this situation is that the wrong atoms have been chosen in *Regularize*. The noise is still the main reason, and the solution way in this algorithm is also a factor. Therefore, the residual in each iteration is saved in this study and the final answer is the one with the smallest residual.

For the third problem, the DMI is the common choice for the classical MP algorithms. However, the system matrix of MFI is so huge that DMI needs huge computational expense. Furthermore, the ill-posed matrix and the noise that existed in structural responses will reduce the accuracy seriously if the DMI is used. Therefore, the least square QR-factorization (LSQR) method,[35] which has been

proven to be an effective way for the ill-posed problem, is chosen to solve Eq. (10) in the process of *Update*.

If $V_k(\beta_1 e_1) = r$, Eq. (10) is transformed into a least squares problem:

$$\min \|\beta_1 e_1 - B_k y_k\|, \tag{12}$$

where the subscript k is the number of steps in LSQR algorithm, β_i and V_k are a scalar and a matrix generated by the Lanczos process, respectively, and B_k is a lower bidiagonal matrix with a dimension of $(k+1) \times k$.[35]

In this method, the initial position of solution $\boldsymbol{x}_0$ is related to the accuracy of results. All of them are settled as zeros at the beginning. With the increase of iteration, the new chosen values related to *Regularize* are still set as zeros and the other values are set as the solution in the last iteration:

$$\begin{cases} \boldsymbol{x}_0 = \boldsymbol{\Theta}, & i = 1, \\ \boldsymbol{x}_0 = \boldsymbol{x}_0 \cup \boldsymbol{\Theta}, & i > 1. \end{cases} \tag{13}$$

Before introduction of prior knowledge, it is noted that the lighter axle-weight is always hard to be accurately identified for multiaxial vehicles. This is because the response caused by the lighter axle is far less than the one by the heavier axle-weight of a vehicle. Therefore, the atom related to the lighter axle is hard to be recognized in *Regularize* at the beginning. Furthermore, the influence of noise makes this problem more difficult. To address this problem, the basis functions related to the static axle-weights of vehicles are chosen at first to obtain the coefficients related to them. Then the initial value should be changed into

$$\boldsymbol{I} = [N_1 N_2 \dots N_{ii}], \quad \boldsymbol{A} = \boldsymbol{\Phi}_N, \quad \boldsymbol{r} = \boldsymbol{Y} - \boldsymbol{A}\boldsymbol{\alpha}_s,$$

where N_{ii} represents the index of the iith static axle-weight of vehicles in the redundant matrix, $\boldsymbol{\Phi}_N = [\boldsymbol{\Phi}_1 \boldsymbol{\Phi}_2 \cdots \boldsymbol{\Phi}_{ii}]$, $\boldsymbol{\Phi}_{ii}$ indicates the basis function related to the iith static axle-weight in the redundant matrix. The axle number in this study is set as ii. $\boldsymbol{\alpha}_s$ is the coefficient related to static axle-weight in the first solution. The elements related to $\boldsymbol{\Phi}_N$ in $\boldsymbol{\Phi}$ should also be set as zeros after constructing the update matrix $\boldsymbol{A}$: $\boldsymbol{\Phi}_N = \boldsymbol{\Theta}$.

The $\boldsymbol{\alpha}_s$ is also set as the initial position $\boldsymbol{x}_0$ in the LSQR algorithm at first, then Eq. (13) should be modified as follows:

$$\begin{cases} \boldsymbol{x}_0 = \boldsymbol{\alpha}_s, & i = 1, \\ \boldsymbol{x}_0 = \boldsymbol{x}_0 \cup \boldsymbol{\Theta}, & i > 1. \end{cases} \tag{14}$$

It should be noted that $\boldsymbol{\alpha}_s$ will be changed in each iteration and be more accurate with the increase of iterations due to the choice of different index sets. According to the discussion in Sec. 2.2, in addition to the coefficients related to the static axle-weight, the other coefficient $\boldsymbol{\alpha}_i$ should be smaller than the related coefficient $\boldsymbol{\alpha}_s$, their relationship is related to road roughness, vehicle–bridge characteristics and so on. Therefore, a coefficient ε_3 is introduced to describe it. If

$$\boldsymbol{\alpha}_i < \varepsilon_3 \boldsymbol{\alpha}_s,$$

its related parameter in index set $\boldsymbol{I}$, the update matrix $\boldsymbol{A}$ and itself in $\boldsymbol{\alpha}_i$ will be deleted:

$$\boldsymbol{I}_k = [\,], \quad \boldsymbol{A}_k = [\,],$$

where $\boldsymbol{I}_k$ and $\boldsymbol{A}_k$ represent the kth element in $\boldsymbol{I}$ and the kth column vector in $\boldsymbol{A}_k$, respectively. $[\,]$ indicates empty set. This modification ensures that the coefficients related to the other basis functions will be smaller than the ones related to the static axle-weight of vehicles, which agrees with the prior knowledge adopted.

It is noted that these deleted coefficients will be changed with the increase of chosen atom. However, the column vector related to the deleted coefficient in $\boldsymbol{\Phi}$ has been converted into a vector with all zero elements, which means that the basis functions related to them will be ignored in the following iteration. Therefore, these column vectors in $\boldsymbol{\Phi}$ will be recovered to ensure the accuracy of MFI results.

To summarize, the determination of new parameters based on prior knowledge and the flow chart of the proposed NRAMP method for MFI are shown in Figs. 2 and 3, respectively. The satisfactory criteria in Fig. 3 are related to the adaptive process about ε_1 and ε_2. Through these improvements, the unknown sparsity problem can be solved, and the solution will have stronger robustness and higher coincidence with the prior knowledge of moving forces. The computation cost of this method will be reduced compared with the other OMP methods especially in the following experiment.

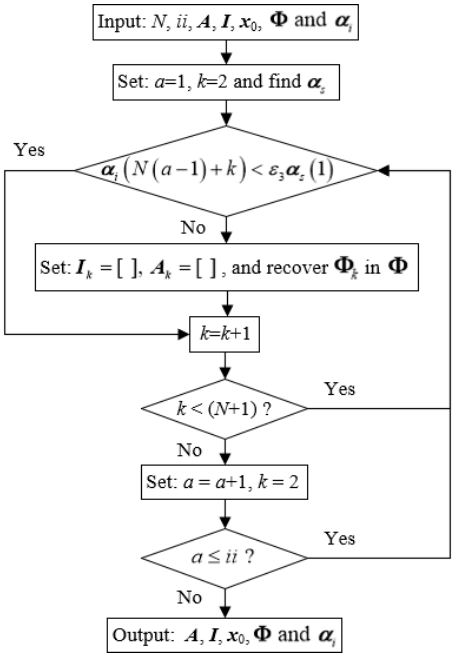

Fig. 2. Determination of new parameters based on prior knowledge.

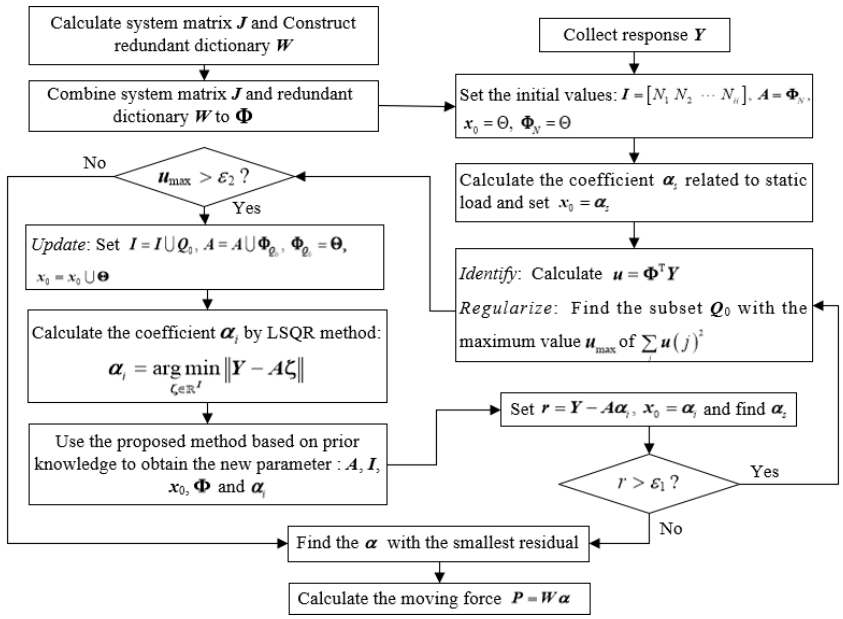

Fig. 3. Flow chart of proposed NRAMP for MFI.

3. Numerical Simulations

3.1. *Simulation setup*

To assess the feasibility of the proposed NRAMP, some numerical simulations on MFI are carried out below. The highest interested frequency of the moving forces is $f_r = 50\,\text{Hz}$ and $T = 1\,\text{s}$, then the number of basis functions is 301 for each moving force according to Eq. (5). Two typical simulations of moving forces are considered:

(a) single moving force with impulse components

In practice, moving vehicle loads usually contain impulse components due to puddles, expansion joints and speed bumps on bridge decks, which are hard to identify accurately, particularly in the impulse peak and at moment.[14,36] To validate the proposed NRAMP and simulate the real environment, an expansion joint at the 3/5 span of the beam is considered in Eq. (15)[24]:

$$P_1(t) = \begin{cases} 40[1 + 0.3\sin(25\pi t) + 0.2\sin(60\pi t)]\,\text{kN} & 0\,\text{s} \le t < 0.6\,\text{s} \\ 40[1 + 0.3\sin(25\pi t) + 0.2\sin(60\pi t) & \\ \quad + 3e^{-35(t-0.6)}\sin(125(t-0.6))]\text{kN} & 0.6\,\text{s} \le t < 1\,\text{s} \end{cases} \tag{15}$$

(b) two unequal moving forces

This model always leads to the fact that the identified result of the heavier axle-weight is more accurate than the lighter axle-weight especially in high noise level.[36]

Their specific forms are in the following form:

$$\begin{cases} P_1(t) = 5[1 + 0.1\sin(10\pi t) + 0.05\sin(40\pi t)]\,\text{kN}, \\ P_2(t) = 20[1 - 0.1\sin(10\pi t) + 0.05\sin(50\pi t)]\,\text{kN}. \end{cases} \tag{16}$$

The speed v of these moving forces is 40 m/s, and the distance between two moving forces is 4 m. The parameters of the bridge are considered as follows: the span of the beam is $l = 40\,\text{m}$, the density of unit length is $\rho = 12000\,\text{kg}\cdot\text{m}^{-1}$ and the flexural rigidity is $\text{EI} = 1.275 \times 10^{11}\,\text{N}\cdot\text{m}^2$. Furthermore, the first three vibration modes are used in the MFI computation and the corresponding damping ratios are set to 0.02, 0.02 and 0.04, respectively. The sampling frequency of structural responses is set to 200 Hz.[10]

For simulating the polluted responses in practice, random noise is added to the calculated response $\boldsymbol{R}_{\text{calculated}}$ to simulate the measured responses $\boldsymbol{R}_{\text{measured}}$ as follows[24]:

$$\boldsymbol{R}_{\text{measured}} = \boldsymbol{R}_{\text{calculated}} + \boldsymbol{N}_{\text{oise}} \times \frac{1}{N_r}\sum_{i=1}^{N_r} |\boldsymbol{R}_i| \times \text{rand}, \tag{17}$$

where $\boldsymbol{N}_{\text{oise}}$ and rand represent noise levels ranging from 0 to 1 and a standard normal distribution vector with zero mean value and unit standard deviation, respectively. N_r is the element number of vector $\boldsymbol{R}_{\text{calculated}}$.

To assess the accuracy of the proposed method, the relative percentage error (RPE) between the identified and true moving forces is defined as

$$\text{RPE} = \frac{\|\boldsymbol{P}_{\text{true}} - \boldsymbol{P}_{\text{identified}}\|}{\|\boldsymbol{P}_{\text{true}}\|} \times 100\%, \tag{18}$$

where $\boldsymbol{P}_{\text{true}}$ and $\boldsymbol{P}_{\text{identified}}$ are the true and identified forces, respectively.

For the LSQR method employed in the proposed method, the tolerance and the maximum iterations are settled as 10^{-6} and 100, respectively. The initial position is a vector composed of zeros. For the stop criteria of the proposed method as mentioned in Sec. 2.3, ε_1 and ε_2 are set as 10^{-6} and 10^{-10}, respectively, and the ε_3 is set as 0.5.

In the following tables and figures, 'm' and 'a' represent bending moment and acceleration responses, respectively. '1/4', '1/2' and '3/4' represent the locations of sensors in the span of bridge. For example, '1/4a' represents that the acceleration response collected from an accelerometer located at 1/4 span of bridge is adopted to execute the MFI calculation. The computer configuration in numerical simulations is as follows: Windows 10 Professional version system, intel(R) Core (TM) i7-6700HQ CPU @ 2.60 GHz, 8.00 GB (RAM) memory, Nvidia Geforce GTX950M (2 GB LENOVO) graphics card.

3.2. *Identification of single moving force with impulse components*

In this part, the moving force in Eq. (15) is set as the true force. Both bending moment response at 1/4 span and acceleration response at 1/2 span are used for MFI.

Three noise levels, i.e. 5%, 10% and 15% are adopted in this study. Comparison of MFI results under different noise levels are shown in Fig. 4. It can be found that the proposed NRAMP has a strong robustness, and the local impulse peak and at moment of 0.6 s can be identified accurately.

To make the comparison more persuasive, both the orthogonal matching pursuit (OMP) and regularized OMP (ROMP) algorithms are used to conduct. The maximum iterations of these methods are set as half of the element number of coefficient vector. Furthermore, if the norm of the residual in each iteration is smaller than $\varepsilon_1 = 10^{-6}$, these algorithms can stop. For the ROMP algorithm, the maximum energy is smaller than $\varepsilon_2 = 10^{-10}$, the algorithm can also stop. The comparison of RPE values by different methods is listed in Table 1.

It can be seen that the proposed NRAMP method has a better MFI accuracy than the other two OMP methods from either in the RPE values of static axle-weights or

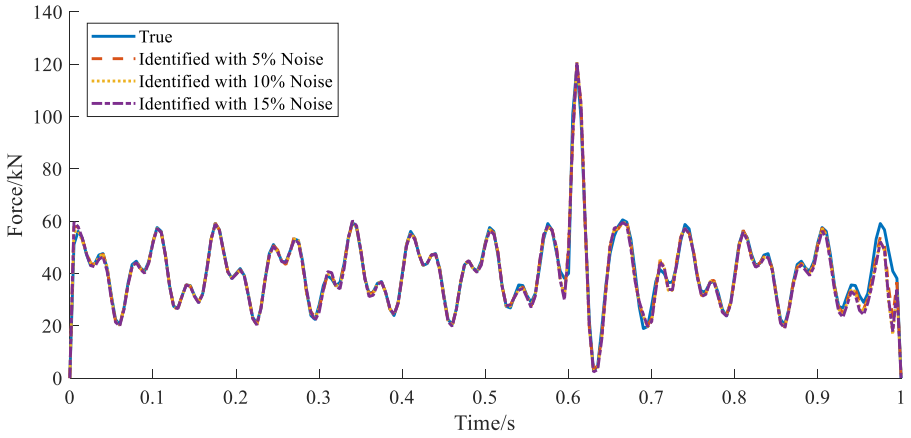

Fig. 4. Comparison of MFI results using 1/4 m&1/2a under different noises.

Table 1. Comparison of RPE values by different methods.

		Relatively percentage error (RPE)/%		
Methods	Noise level	Static axle-weight	GVW	Executive time/s
OMP	5%	64.03	6.48	0.15
	10%	36.41	8.84	0.14
	15%	61.10	11.03	0.14
ROMP	5%	†	†	0.66
	10%	†	†	0.67
	15%	†	†	0.77
Proposed	5%	2.42	5.55	0.17
	10%	2.03	6.90	0.14
	15%	1.10	7.19	0.16

Note: † represents RPE value larger than 1 000% and GVW indicates gross vehicle weight.

in ones of GVWs obviously, in which the ROMP method is even failed since all the RPE values are higher than 1 000% for both static axle-weight and GVWs under different noises. For the OMP method, even though the RPE values of GVWs are relatively smaller, the RPE values for static axle-weights are unacceptable under different noises, where the smallest RPE value of them reaches up to 36.41%, which shows that the OMP method cannot effectively identify the static axle-weight under different noises. But for the proposed NRAMP method, the RPE values of static axle-weights are kept under 3% even the noise level is 15%. Furthermore, from the view of computational expenses, both the proposed method and OMP algorithm are in the same order. They are both kept in 0.2 s. For the ROMP algorithm, its computational expense is the worst among the three methods.

Under 15% noise level, a comparison of MFI results by three methods is shown in Fig. 5. It can be seen that the ROMP result is in failure because it heavily deviated from the true force. For the OMP algorithm, especially for each peak value of dynamic load components, the identified result does not correspond to the true force. For example, the MFI results near the moments of 0.27 s and 0.79 s by the OMP method are worse than that due to the NRAMP method obviously. Furthermore, even though the identified results between the OMP and NRAMP methods are close to each other in time domain, the RPE value for the static axle-weight (P_1) by the

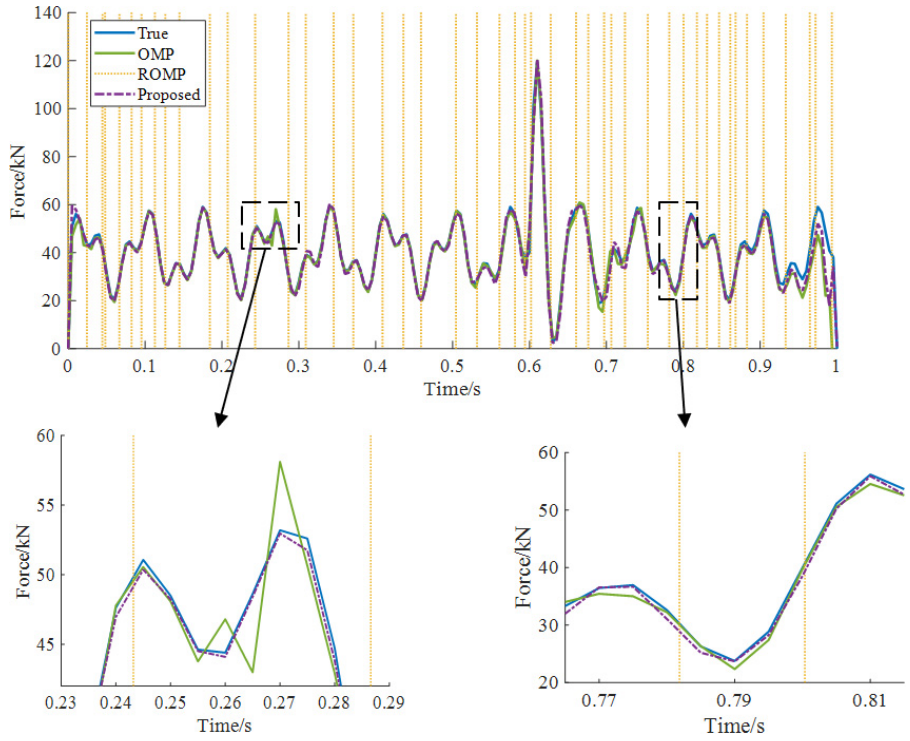

Fig. 5. Comparison of MFI results using 1/4m&1/2a under 15% noise level.

OMP, which is related to the first atom in the redundant matrix, is much worse than that by the NRAMP as in Table 1. As a result, it can be found that the proposed NRAMP method is more suitable in MFI. However, the identified values near the support ends of the bridge still deviate a little from the true force, although they are better than the ones by the other OMP methods. This shows that the local impulse has a great impact on the method especially for the identification of the moments when the vehicle leaves or arrives at the beam. This is because the identifications at these moments are the impulse components in the moving force. The rectangular function is sensitive to them especially since there is also another bigger impulse component in the moving force. To accord with the response caused by expansion joint, the rectangular function will try to make the real signal energy tend to average within the response time, which leads to lower identification amplitude at these moments.

3.3. *Identification of two unequal moving forces*

To further assess the availability of the proposed NRAMP method, Eq. (16) has been adopted in this part. More response combinations are set to make the conclusion more persuasive. The noise level is set as 10%. Similarly, both the OMP and ROMP algorithms have been chosen to compare with the proposed method. The stop iterations are set as the same as the ones in the section of single moving force simulation. As a result, the RPE values of these methods are listed in Table 2. A comparison of MFI results from the response combinations '1/4m&1/2a&3/4a' under 10% noise is shown in Fig. 6.

From Table 2, it can be found that the RPE values by the proposed NRAMP are kept under 4.16%, which are greatly more accurate compared with the ones by both OMP and ROMP algorithms. Moreover, the RPE values in first lighter-axle are always higher than the ones in the second heavier-axle. This is because the first axle-weight is lighter than the second ones so the responses caused by the lighter axle-weight are affected by the noise more easily. However, compared with two OMP methods, the MFI accuracy in the lighter axle by the proposed NRAMP is still more accurate. Under the case of '1/4a&1/2m&3/4a', it can be found that the RPE values

Table 2. Comparison of RPE values by different methods under 10% noise.

	OMP		ROMP		Proposed		Executive time/s		
Response combinations	P_1	P_2	P_1	P_2	P_1	P_2	OMP	ROMP	Proposed
1/4m&1/2a	142.0	161.9	885.4	299.6	4.16	1.35	1.47	0.53	0.16
1/2m&1/2a	108.1	80.61	17.98	11.31	4.10	1.46	1.31	0.03	0.13
1/4m&1/2a&3/4a	179.0	35.08	17.89	3.38	1.20	0.68	1.59	0.05	0.33
1/4m&1/2m&3/4a	77.28	36.68	†	640.9	1.57	0.86	1.44	0.89	0.31
1/4a&1/2m&3/4a	†	174.1	†	301.1	3.39	1.10	1.36	0.75	0.39

Note: † represents RPE value larger than 1 000%.

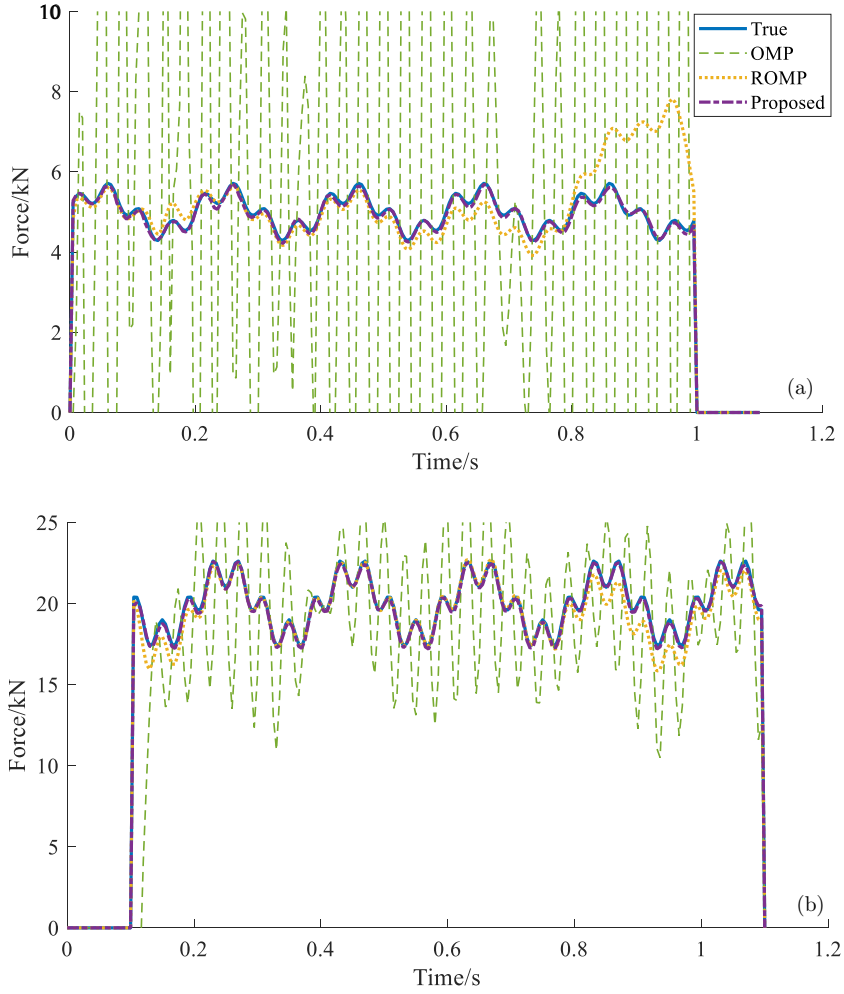

Fig. 6. Comparing on MFI results from 1/4m&1/2a&3/4a under 10% noise: (a) first axle and (b) second axle.

in first axle by both the OMP and ROMP methods are higher than 1 000%, but the one by the proposed NRAMP is only 3.39%.

Compared with MFI results on numerical simulations in single time-varying moving force, it can be found that the accuracy of the OMP algorithm has been reduced seriously. From Fig. 6, the fluctuations of the MFI results by the OMP are substantial, especially for the first lighter axle. Furthermore, it can be found from Table 2 that the executive times for the OMP are greatly increased compared with the ones for both the ROMP and proposed NRAMP method. This is because there are two redundant matrixes in Eq. (2), in which there is a significant influence on the calculation of coefficients related to the lighter axle in Eq. (4). For the ROMP method, it can be found that the RPE values are almost acceptable under the

response combinations of '1/2m&1/2a' and '1/4m&1/2a&3/4a'. From Fig. 6, it can be found that there are significant errors between amplitudes of moving forces identified by the ROMP method and true ones, especially for the first lighter axle when the axle leaves the bridge. Compared with the MFI results in single time-varying force simulations, the local impulse has a great impact on this method.

For the executive time, it can be found from Table 2 that the proposed NRAMP method is related to the number of chosen responses. Compared with the two OMP methods, it is more stable in a way. Furthermore, its executive times are far less than the OMP method. Even though they are longer than the ROMP's executive times in the response combinations of '1/2m&1/2a' and '1/4m&1/2a&3/4a', they are less than the ROMP's times in other response combinations. In a short, the proposed NRAMP method not only has the highest MFI accuracy but also almost the lowest computational expense in all the three methods.

Appropriate choices of multiple criteria coefficients ε_2 and ε_3 are important to the successful application of the proposed method. Then the effect of different choices of ε_2 and ε_3 on the MFI results is discussed below. Here, it is unnecessary to discuss the ε_1, since it is the relative error between ones in two successive iteration steps, the default satisfies the requirement of accuracy. Table 3 lists the RPE values under different choices of ε_2 and ε_3 using response combination '1/4a&1/2m&3/4a' under the noise level of 10%. It can be found that these parameters have an impact on the MFI results. With the decrease of ε_3, the RPE values are relatively larger. This situation is more obvious for the lighter axle (P_1). The effect of ε_2 on RPE values is relatively small, but it can be found that the identified results may not be better when ε_3 is small. This is because the more chosen atoms are, the more effect of noise on the MFI results is. Furthermore, it can be found that the amplitudes of sine functions are not larger than 0.1 in Eq. (16). Due to the influence of noise on responses, the identified results under $\varepsilon_3 = 0.1$ will be relatively worse.

In short, the proposed NRAMP has strong robustness and better efficiency compared with the existing OMP and ROMP methods. It is reasonable to consider prior knowledge of the ROMP method. It not only saves the executive time of the ROMP method but also improves the accuracy of the matching pursuit algorithm, either in the identification of local impulse moving force or in two unequal moving forces. For the selection of multiple-criteria coefficients in the proposed NRAMP, the larger ε_3 related to prior knowledge is chosen, the best identification can be obtained. Even though the ε_2 related to *Regularize* has a little impact on the MFI results, a

Table 3. Comparison of the effect of different choices of ε_2 and ε_3 on RPE values.

	$\varepsilon_3 = 0.8$	$\varepsilon_3 = 0.5$	$\varepsilon_3 = 0.3$	$\varepsilon_3 = 0.1$
$\varepsilon_2 = 10^{-10}$	1.57(0.50)	3.39(1.10)	4.75(1.70)	8.80(1.77)
$\varepsilon_2 = 10^{-7}$	1.57(0.50)	3.39(1.10)	4.75(1.70)	8.80(1.77)
$\varepsilon_2 = 10^{-4}$	1.57(0.50)	2.59(0.90)	2.72(0.60)	8.80(1.77)

Notes: Values in underlined "_" and and in parenthesis "()" are for P_1 and P_2, respectively.

relatively higher value is the better choice which shows the best in different sets of ε_3. In this study, $\varepsilon_2 = 10^{-4}$ and $\varepsilon_3 = 0.8$ is the optimal allocation.

4. Experimental Verifications

4.1. *Experimental setup*

To further assess the reliability of the proposed NRAMP method, a bridge–vehicle model is designed and fabricated in the laboratory, as shown in Fig. 7(a), where a model vehicle is moving on a hollow thin-wall beam.

The section form of main beam is rectangle, its width, height, wall thickness and span are 0.15 m, 0.05 m, 0.002 m and 3 m, respectively. Its density of unite length and flexural rigidity are $\rho = 7.62467\,\mathrm{N}\cdot\mathrm{m}^2$ and $\mathrm{EI} = 7.9432 \times 10^4\,\mathrm{N}\cdot\mathrm{m}^2$, respectively. The model car is shown in Fig. 7(b) with a wheelbase of 0.33 m. It is pulled by a motor ahead through a traction rope. The car will be accelerated on the leading beam when the motor starts. When the car is moving on the main beam, its velocity shall be as unchanged as possible. After the car exits the main beam, the motor will be turned off to simulate the vehicle slowing down until stopping on the trailing beam. This measure can also prevent the car against rushing out of the bridge deck in a high speed.

Before analyzing the data, the support conditions as shown in Fig. 7(c), and the material parameters of bridges need to be carefully considered due to pedestal looseness and material corrosion. Therefore, an experimental modal analysis (EMA) is conducted firstly.[37] The first three measured frequencies, which are 19.45 Hz,

Fig. 7. Experimental setups. (a) Experimental beam, (b) model car, (c) support end and (d) shaker.

72.43 Hz and 162.01 Hz, respectively, are measured for MFI computation. Their corresponding damping ratios are 1.41%, 1.44% and 0.58%, respectively. Due to the fact that the ideal hinge supports are impossible in practice, the original FE model of the main beam should be updated firstly. The main objective of FE model updating is to find reasonable physical parameters of the model by minimizing the modal parameters between the FE analysis and the EMA. In this study, the first three natural frequencies and mode shapes are used to update the FE model with 20 beam elements as shown in Fig. 8, the vertical spring coefficients kv and rotational spring stiffness kr are updated. The particle swarm optimizer (PSO) algorithm,[37] which has been used widely, is introduced here to update the FE model. Finally, the relative error between the measured natural frequency f_m and updated one f_u, and the modal assurance criterion (MAC) values between each measured mode shape $\boldsymbol{\varphi}_m$ and corresponding calculated one $\boldsymbol{\varphi}_c$ are listed in Table 4 after the model updating. The vertical spring stiffness coefficients of the two support ends are determined as $kv_1 = 8.25 \times 10^8\,\mathrm{N \cdot m^{-1}}$ and $kv_2 = 8.14 \times 10^8\,\mathrm{N \cdot m^{-1}}$, respectively. The rotational spring stiffness coefficients are set as $kr_1 = 1.05 \times 10^4\,\mathrm{N \cdot m^{-1}}$ and $kr_2 = 1.79 \times 10^4\,\mathrm{N \cdot m^{-1}}$, respectively. Through the updated FE model, the first three natural frequencies are calculated and modified as 19.56 Hz, 73.09 Hz and 162.30 Hz, respectively. To a certain extent, the modified frequencies are in good agreement with the measured ones.

To estimate the speed of model vehicle, seven photoelectric sensors are installed near the main beam. The moments that the axles of the model vehicle go through them can be accurately obtained. The distance between two consecutive sensors is 0.5 m equally, as shown in Fig. 7(a), the sudden impulse change of signal means that one of vehicle axles is passing through the photoelectric sensor. The same time intervals between two consecutive photoelectric sensors means that the velocity of vehicle is assumed as unchanged on the bridge.[23,38] However, in practice, there are still some differences in each interval. For this experiment, this is because the winding diameter of traction rope on the spindle of motor is getting larger and larger,

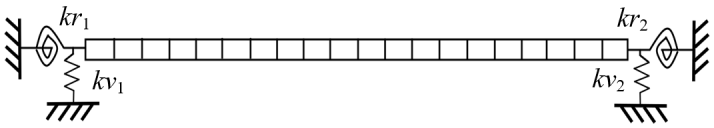

Fig. 8. Finite element model of main beam.

Table 4. Comparison of the first three modal parameters.

	Frequencies (Hz)		Error (%)	MAC
Modes	f_m	f_u	$\lvert f_m - f_u\rvert / f_m$	$(\boldsymbol{\varphi}_m^T \boldsymbol{\varphi}_c)^2 / (\boldsymbol{\varphi}_m^T \boldsymbol{\varphi}_m)(\boldsymbol{\varphi}_c^T \boldsymbol{\varphi}_c)$
1st	19.45	19.56	0.57	0.9877
2nd	72.43	73.09	0.91	0.9753
3rd	162.01	162.30	0.18	0.8999

which makes the vehicle velocity faster and faster. Therefore, the velocity is assumed to be changed in the whole duration but unchanged in the interval between each two adjacent photoelectric sensors. It has a direct impact on the construction of system matrix in Eq. (3). To better distinguish velocity situations, the average velocity v_0 is still set as indicators of different velocity situations in the following. Some typical measured signals from photoelectric sensor, strain gauge and accelerometer are shown in Fig. 9 when the model vehicle with GVW = 11.1388 kg moves on the main beam at a speed of $v_0 = 1.2427$ m/s.

Three strain gauges are installed at 1/4, 1/2 and 3/4 span of the bridge, respectively. Before data collection, the relationship between the measured data and their related bending moment needs to be calibrated. Five-level masses are placed at 1/4, 1/2 and 3/4 span of the bridge successively. Each level is 49.98 N. Two of their

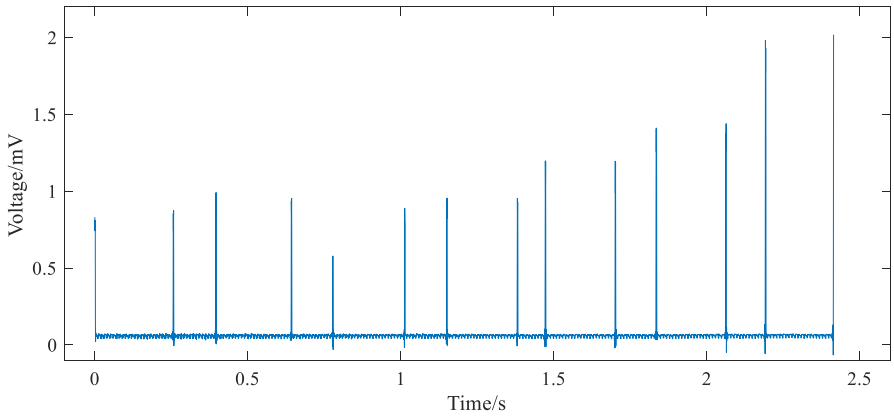

(a)

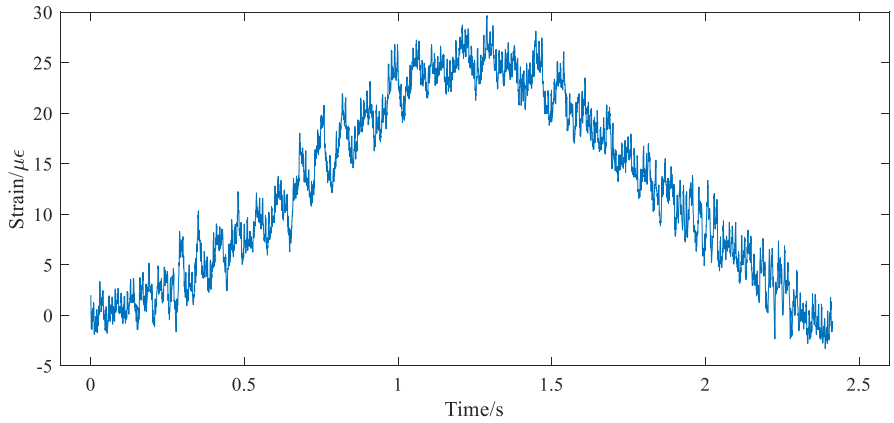

(b)

Fig. 9. Typical measured signals from (a) photoelectric sensor, (b) strain gauge and (c) accelerometer.

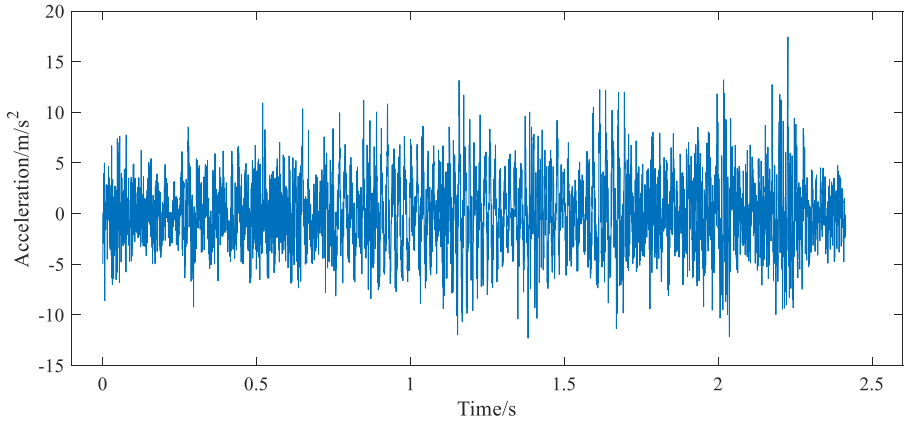

(c)

Fig. 9. (*Continued*)

relationships between measured strain and calculated bending moment are shown in Fig. 10. It can be found that they satisfy the linear relationship in all cases. For the collection of acceleration responses, seven acceleration sensors (PCB, ICP333B30) at 1/8, 1/4, 3/8, 1/2, 5/8, 3/4 and 7/8 span are installed on the bridge. The sampling frequency is 2 048 Hz when the LMS Test.Lab is employed for data collection and analysis.

A low-pass Butterworth filter with no more than 3 dB of passband ripple and at least 40 dB of attenuation in the stopband is used to filter all the responses. Considering the truth that the third mode shape of vertical vibration is 162.01 Hz, the edges of its passband and stopband are 165 Hz and 230 Hz, respectively. For easy storage and convenient calculation, all the filtered data including the strain response

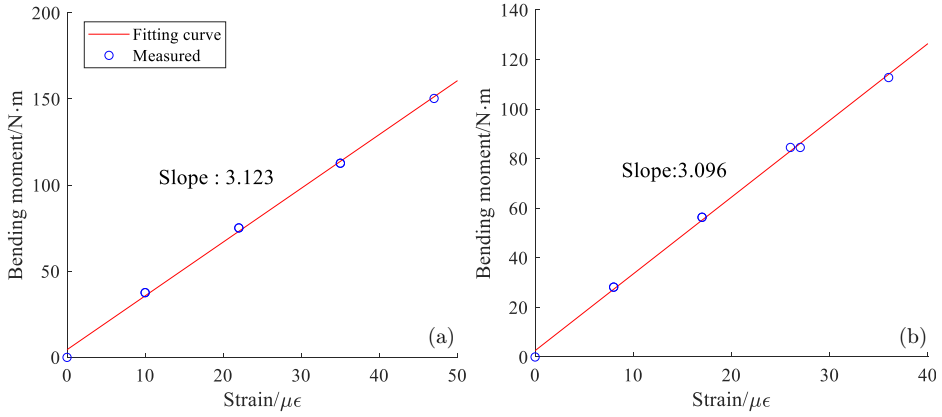

Fig. 10. Calibration coefficients between measured strain responses and corresponding calculated bending moments. (a) 1/2 span and (b) 3/4 span.

and the acceleration response are resampled at 512 Hz. In this study, all the measured responses are firstly recorded at a sampling rate of 2 048 Hz, which is for meeting the requirements of higher frequency components in another study purpose simultaneously, and then resampled to form the response data at a sampling rate of 512 Hz for this MFI problem. Because the first three frequencies of the main beam are 19.45 Hz, 72.43 Hz and 162.01 Hz, respectively, according to the Shannon sampling theorem, all the response data recorded at a sampling rate of 512 Hz are enough for MFI in this experiment. With the utilization of filters, the responses have been delayed, and they should be modified by deleting the first few data of the filtered responses and adding the same number of the original responses in the last. Furthermore, alternating current oscillates at a multiple of 50 Hz, these oscillations usually destroy the measured responses and must be subtracted.

Several response combinations with different GVWs and mean velocities have been chosen to assess the effectiveness of the proposed NRMAP method. The identified static axle-weight is chosen to assess due to the fact that the real moving force is unknown, but the real static axle-weight is known. Then the RPE of axle-weight is defined as

$$\mathrm{RPE}w = \frac{|w_{\mathrm{iden}} - w_{\mathrm{true}}|}{w_{\mathrm{true}}} \times 100\%, \tag{19}$$

where w_{iden} and w_{true} are the identified axle-weight by the proposed method and true axle-weight, respectively.

In this experiment, the highest interested frequency is assumed as $f_r = 250$ Hz. The multiple-criteria coefficients ε_1 and ε_2 related to the stop iterations and the ε_3 related to the prior knowledge are set as the same as the ones in the numerical simulations. The OMP and ROMP methods are also compared here. Table 4 lists the RPEw of different methods based on the response combination 1/2m&3/4m&3/8a and mean vehicle velocity 1.2427 m/s. The front and rear axle-weights are 5.5671 kg and 5.5717 kg, respectively. From Table 5, it can be found that the identified results by the OMP and ROMP methods derivate from the true axle-weight seriously especially for the ROMP method. The front axle-weight identified by the OMP method is even a negative value. But for the proposed NRAMP method, the RPEw of the front and rear axle-weights is only 8.46% and 1.75%, respectively. Furthermore, the executive time of the OMP method is more than half an hour. But the executive time of the proposed method is only 1.10 s which is far less than the ones due to the OMP

Table 5. Identified results by different methods under 1/2m&3/4m&3/8a.

Methods	Front axle (unit: kg) identified (True)	Rear axle (unit: kg) identified (True)	Executive time/s
OMP	−410.80 (5.5671)	57.97 (5.5717)	2 709.92
ROMP	4.01×10^7 (5.5671)	3.67×10^3 (5.5717)	80.94
Proposed	5.0960 (5.5671)	5.6691 (5.5717)	1.10

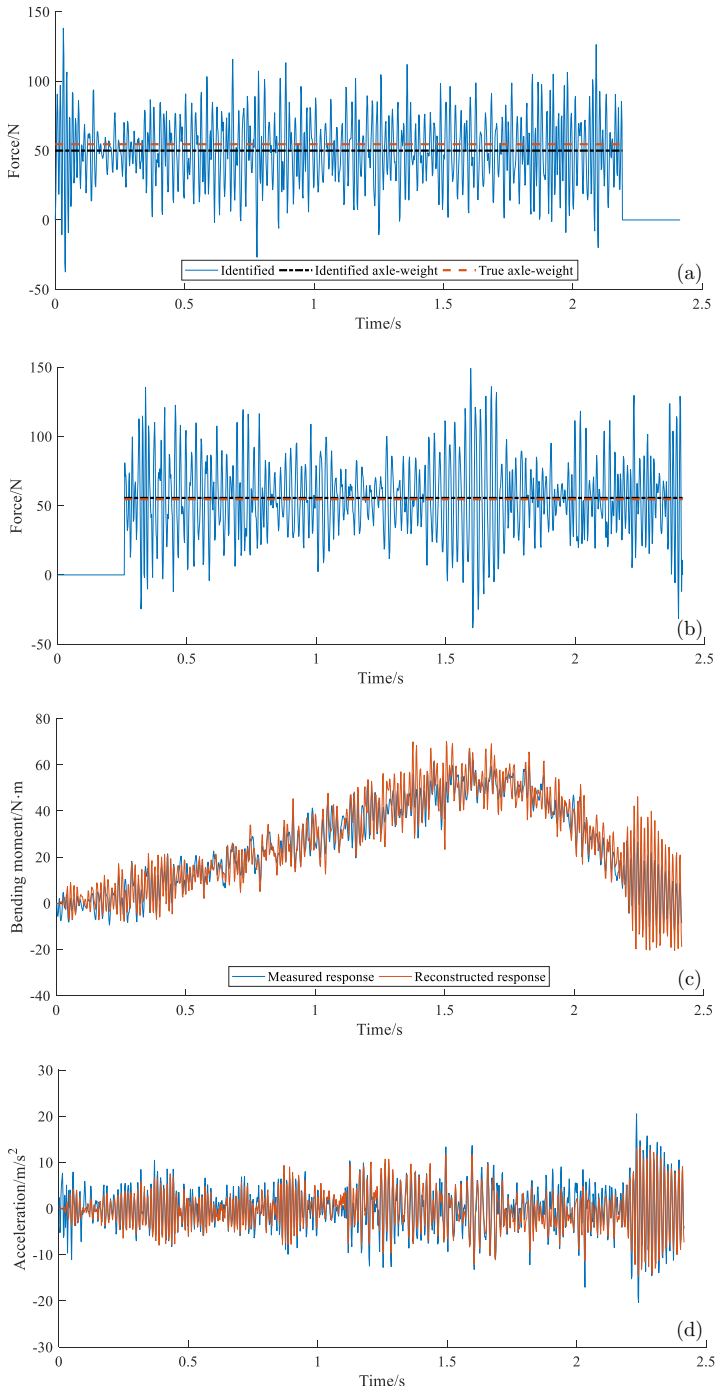

Fig. 11. MFI results under response combination 1/2m&3/4m&3/8a and vehicle velocity 1.2427 m/s. (a) Front axle, (b) rear axle, (c) 3/4m and (d) 3/8a.

and ROMP methods. The identified results by the proposed NRAMP method are shown in Fig. 11, it can be found that the identified force is fluctuate around the true static axle-weight. Even though the RPEw of GVW is only 3.35%, the identified front axle-weight has a higher deviation from the true axle-weight compared with the error in the rear axle-weight due to the noise in the measured responses. Furthermore, both the bending moment and acceleration responses are reconstructed from the moving forces identified by the proposed NRAMP method and compared with the measured ones as shown in Figs. 11(c) and 11(d), respectively. It can be seen that the reconstructed responses conform to the measured ones greatly, which shows that the MFI results by the proposed method are reasonable and acceptable.

To make the proposed method more convincible, more situations are considered. Table 6 lists the MFI results by the proposed NRAMP method under different velocities. Even though the identified results of the rear axle under the velocity of 0.7178 m/s are relatively worse, the RPEw of GVW is only 3.59%. It can be found that under different velocities, the RPEw of GVW can be still controlled under 3.6%. Table 7 also lists the MFI results by the proposed NRAMP method based on the response combination 1/2m&3/4m&3/8a under different axle-weights. It can be found that all the RPEw have been controlled in a relatively small range. Especially for the identification of the lighter axle-weight which is a tricky problem, its RPEw is controlled under 10%. Table 8 lists the identifications under the GVW of 11.7410 kg and the mean vehicle velocity of 0.5434 m/s based on response combinations. The identified results show that the proposed NRAMP method can obtain an accurate result even though only two response sensors are used.

Table 6. Identified results by the proposed method under different velocities.

Mean velocity (unit: m/s)	Front axle (unit: kg) identified (True) RPEw	Rear axle (unit: kg) identified (True) RPEw	GVW (unit: kg) identified (True) RPEw
1.2427	5.0960 (5.5671)	5.6691 (5.5717)	10.7651 (11.1388)
	8.46%	1.75%	3.35%
0.7178	5.1756 (5.5671)	6.3635 (5.5717)	11.5391 (11.1388)
	7.03%	14.24%	3.59%
0.3444	5.0560 (5.5671)	5.8627 (5.5717)	10.9187 (11.1388)
	9.18%	5.22%	1.98%

Table 7. Identified results by the proposed method under different axle-weights.

Mean velocity (unit: m/s)	Front axle (unit: kg) identified (True) RPEw	Rear axle (unit: kg) identified (True) RPEw	GVW (unit: kg) identified (True) RPEw
1.2427	5.0960 (5.5671)	5.6691 (5.5717)	10.7651 (11.1388)
	8.46%	1.75%	3.35%
1.2402	6.0191 (6.6510)	5.5262 (5.1842)	11.5453 (11.8352)
	9.50%	6.60%	2.45%
1.1972	4.7098 (4.9669)	7.2441 (6.7741)	11.9539 (11.7410)
	5.18%	6.94%	1.81%

Table 8. Identified results by the proposed method under different response combinations.

Response combinations	Front axle (unit: kg) identified (True) RPEw	Rear axle (unit: kg) identified (True) RPEw	GVW (unit: kg) identified (True) RPEw
3/4m&3/8a	5.2338 (4.9669) 5.37%	6.5289 (6.7741) 3.62%	11.7627 (11.7410) 0.18%
3/4m&5/8a	4.9001 (4.9669) 1.34%	6.8132 (6.7741) 0.58%	11.7133 (11.7410) 0.24%
3/4m&5/8a&1/4a	4.8608 (4.9669) 2.14%	6.6471 (6.7741) 1.87%	11.5079 (11.7410) 1.99%

5. Conclusions

In this study, a novel regularized adaptive matching pursuit (NRAMP) is proposed to improve the ill-posedness, executive efficiency and accuracy in the moving force identification (MFI) problem. At first, the MFI problem is converted into a sparse recovery problem with redundant matrixes. Based on some adaptive criteria, the problem of unknown sparsity of moving force has been solved. Then the LSQR method is used instead of direct matrix inversion (DMI) in each iteration to address the ill-posedness of system matrix. Another criterion, which is related to the prior knowledge that static component is main part in the moving force, is also used to pick the reasonable atom in each iteration, where each MFI result is related to the minimum residual in all iterations. Finally, numerical simulations on identification of one single moving force with impulse components and two unequal moving forces, and experimental verifications on MFI of a model vehicle crossing a beam in laboratory are carried out to validate the feasibility of the proposed NRAMP. From these results, some conclusions can be made as follows:

(1) Compared with the OMP and ROMP methods, the proposed NRAMP has dealt with unknown sparsity and ill-posed problems perfectly. It has higher accuracy and strong robustness in all simulation cases. Not only the impulse peak and at moment in single moving force but also the lighter axle-weight in two unequal moving forces can be identified accurately by the proposed NRAMP. The proposed method can perform well even under the higher noise level 15%.
(2) The executive times by the proposed method are much less than that due to the common OMP methods in most cases. This phenomenon will be more obvious in experiments. The executive time of the proposed NRAMP is only 1.10 s but the ones due to the OMP and ROMP methods are 2 709.92 s and 80.94 s, respectively, as listed in Table 5.
(3) The proposed NRAMP provides a good potential resolution to the MFI problem. The identified results agree with the prior knowledge that the time-varying components fluctuate around the static axle-weight of a vehicle. The gross vehicle weight of a vehicle can also be identified accurately with a higher MFI accuracy, which is kept under 3.6% in all measured cases by the proposed NRAMP. Furthermore, the MFI results for a vehicle with two axles can also be

obtained accurately if only two bridge response sensors are used, as listed in Table 8.

(4) Even though the MFI results by the proposed NRAMP are relatively accurate, there is still a lot of research to be done in future. Especially, it would be necessary and significant to assess the adaptabilities of the proposed NRAMP through practical engineering in future.

Acknowledgments

This work was jointly supported by the National Natural Science Foundation of China under grant numbers of 52178290 and 51678278.

References

1. X. Q. Zhu and S. S. Law, Recent developments in inverse problems of vehicle–bridge interaction dynamics, *J. Civ. Struct. Health Monit.* **6**(1) (2016) 107–128.
2. J. Sanchez and H. Benaroya, Review of force reconstruction techniques, *J. Sound Vib.* **333**(14) (2014) 2999–3018.
3. Y. B. Yang, Z. L. Wang, K. Shi, H. Xu and Y. T. Wu, State-of-the-art of the vehicle-based methods for detecting the various properties of highway bridges and railway tracks, *Int. J. Struct. Stab. Dyn.* **20**(13) (2020) 2041004.
4. Y. B. Yang and J. P. Yang, State-of-the-art review on modal identification and damage detection of bridges by moving test vehicles, *Int. J. Struct. Stab. Dyn.* **18**(2) (2018) 1850025.
5. W. Y. He, S. Y. Zhu and Z. W. Chen, A multi-scale wavelet finite element model for damage detection of beams under a moving load, *Int. J. Struct. Stab. Dyn.* **18**(6) (2018) 1850078.
6. Z. W. Chen *et al.*, Damage detection of long-span bridges using stress influence lines incorporated control charts, *Sci. China Technol. Sci.* **57**(9) (2014) 1689–1697.
7. H. C. Zhou *et al.*, Development of moving force identification for simply supported bridges: A comprehensive review and comparison, *Int. J. Struct. Stab. Dyn.* **22**(12) (2022) 2230003.
8. L. Deng and C. S. Cai, Identification of parameters of vehicles moving on bridges, *Eng. Struct.* **31**(10) (2009) 2474–2485.
9. C. O'Connor and T. H. T. Chan, Dynamic wheel loads from bridge strains, *J. Struct. Eng.* **114**(8) (1988) 1703–1723.
10. S. S. Law, T. H. T. Chan and Q. H. Zeng, Moving force identification: A time domain method, *J. Sound Vib.* **201**(1) (1997) 1–22.
11. S. S. Law, T. H. T. Chan and Q. H. Zeng, Moving force identification—A frequency and time domains analysis, *J. Dyn. Sys. Meas. Control* **121** (1999) 394–401.
12. X. Q. Zhu and S. S. Law, Dynamic load on continuous multi-lane bridge deck from moving vehicles, *J. Sound Vib.* **251**(4) (2002) 697–716.
13. X. Q. Zhu, S. S. Law and J. Q. Bu, A state space formulation for moving loads identification, *J. Vib. Acoust.* **128**(4) (2006) 509–520.
14. L. Yu and T. H. T. Chan, Recent research on identification of moving loads on bridges. *J. Sound Vib.* **305**(1–2) (2007) 3–21.
15. A. N. Tihonov, On the solution of ill-posed problems and the method of regularization, *Dokl. Akad. Nauk SSSR* **151**(3) (1963) 501–504.

16. S. S. Law *et al.*, Regularization in moving force identification, *J. Eng. Mech.* **127**(2) (2001) 136–148.
17. X. Q. Zhu and S. S. Law, Moving loads identification through regularization, *J. Eng. Mech.* **128**(9) (2002) 989–1000.
18. H. L. Liu, C. Li and L. Yu, Onsite identification of moving vehicle loads on multispan continuous bridge using both dictionary expansion and sparse regularization, *J. Aerosp. Eng.* **34**(3) (2021) 04021018.
19. J. Li and H. Hao, Substructural interface force identification with limited vibration measurements, *J. Civ. Struct. Health Monit.* **6**(3) (2016) 395–410.
20. B. J. Qiao, X. Chen, X. Luo and X. Xue, A novel method for force identification based on the discrete cosine transform, *J. Vib. Acoust.* **137** (2015) 051012.
21. B. J. Qiao *et al.*, The application of cubic B-spline collocation method in impact force identification, *Mech. Syst. Signal Process.* **64–65** (2015) 413–427.
22. B. J. Qiao *et al.*, Group sparse regularization for impact force identification in time domain, *J. Sound Vib.* **445** (2019) 44–63.
23. Z. H. Zhang, W. Y. He and W. X. Ren, Moving force identification based on learning dictionary with double sparsity, *Mech. Syst. Signal Process.* **170** (2022) 108811.
24. C. D. Pan *et al.*, Moving force identification based on redundant concatenated dictionary and weighted l_1-norm regularization, *Mech. Syst. Signal Process.* **98** (2018) 32–49.
25. B. J. Qiao *et al.*, Sparse deconvolution for the large-scale ill-posed inverse problem of impact force reconstruction, *Mech. Syst. Signal Process.* **83** (2017) 93–115.
26. X. J. Ye and C. D. Pan, Force identification under unknown initial conditions by using concomitant mapping matrix and sparse regularization, *J. Vib. Control* **27**(23–24) (2020) 1524–1536.
27. Y. Q. Bao *et al.*, A sparse l_1 optimization-based identification approach for the distribution of moving heavy vehicle loads on cable-stayed bridges, *Struct. Control Health Monit.* **23**(1) (2016) 144–155.
28. N. Huria and M. Feder, Selecting the LASSO regularization parameter via Bayesian principle, in *2016 IEEE Int. Conf. Science of Electrical Engineering* (2016), pp. 1–5.
29. E. J. Candes and T. Tao, Decoding by linear programming, *IEEE Trans. Inf. Theory* **51**(12) (2005) 4203–4215.
30. J. Liu and K. Li, Sparse identification of time-space coupled distributed dynamic load, *Mech. Syst. Signal Process.* **148** (2021) 107177.
31. D. Needell and R. Vershynin, Uniform uncertainty principle and signal recovery via regularized orthogonal matching pursuit, *Found. Comput. Math.* **9**(3) (2009) 317–334.
32. Z. Z. Yang, Z. Yang and L. H. Sun, A survey on orthogonal matching pursuit type algorithms for signal compression and reconstruction, *Signal Process.* **57**(1) (2009) 4333–4346.
33. W. Q. Huang *et al.*, Sparsity and step-size adaptive regularized matching pursuit algorithm for compressed sensing, in *Joint Int. Information Technology and Artificial Intelligence Conf.*, 2nd edn. (2014), pp. 536–540.
34. M. G. Asogbon *et al.*, GBRAMP: A generalized backtracking regularized adaptive matching pursuit algorithm for signal reconstruction, *Comput. Electr. Eng.* **92** (2021) 107189.
35. C. C. Paige and M. A. Saunders, LSQR: An algorithm for sparse linear equations and sparse least squares, *ACM Trans. Math. Softw.* **8**(1) (1982) 43–71.

36. L. Yu, T. H. T. Chan and J. H. Zhu, A MOM-based algorithm for moving force identification: Part I-Theory and numerical simulation, *Struct. Eng. Mech.* **29**(2) (2008) 135–154.
37. J. Kennedy and R. Eberhart, Particle swarm optimization, in *Proc. of ICNN'95 - Int. Conf. Neural Networks*, Perth, Australia (November 1995).
38. H. L. Liu *et al.*, Compressed sensing for moving force identification using redundant dictionaries, *Mech. Syst. Signal Process.* **138** (2020) 106535.